JOURNAL OF THEORETICAL AND APPLIED MECHANICS
61, 2, pp. 379-393, Warsaw 2023
https://doi.org/10.15632/jtam-pl/163290

APPLICATION OF A RING COUPLED DOUBLE-DUFFING OSCILLATOR TO A SCHEME FOR IDENTIFYING THE COULTER SIGNAL WITH A LOW SNR

Zhijie Zhao, Runcong Liu, Xiaodong Wang

Center of Materials Science and Optoelectronics Engineering, College of Materials Science and Opto-Electronic Technology, University of Chinese Academy of Sciences, Beijing, China

Corresponding author Xiaodong Wang, e-mail: xiaodong.wang@ucas.ac.cn

In order to use chaotic oscillators to identify Coulter signals with a low SNR (SNR$\leqslant$ 0), a Gaussian pulse signal is used to simulate the Coulter signal, and we study the continuous synchronous mutation (CSM) phenomenon of a chaotic ring coupled double-Duffing (RCDD) oscillator to identify the signals. The maximum difference between the two state variables in the oscillator can be used to determine the anti-noise ability of the oscillator and construct a function to identify pulse amplitudes. A Simulink model is constructed to verify that the proposed method can be used to identify pulse amplitudes with a low SNR, which provides an approach for developing a technology of measuring Coulter signals with the low SNR.

Keywords: simulated Coulter signal, pulse signal identification, ring coupled double-Duffing oscillator, chaotic-transient synchronous mutation, continuous synchronous mutation

1. Introduction

In 1953, Coulter W.H. proposed the Coulter Principle when he studied the automatic detection technology of blood cells (Coulter, 1953). The Coulter Principle is also known as the Electric Sensing Zone (ESZ) method, which is an electrical method to measure size and quantity of microparticles by detecting pulse signals named Coulter signals. Based on the principle, an instrument named Coulter counter was designed and manufactured. Researchers at McGill University skillfully used the Coulter Principle for reference and proposed to apply it to detect inclusions in a liquid metal. The instrument related to this technology is called Liquid Metal Cleanliness Analyzer (LiMCA) (Doutre, 1984). Because pulse signals measured in the instruments directly reflect the information of microparticles or inclusions, whether the signals can be measured accurately is an important index to evaluate quality of the instruments. In a harsh industrial environment, strong ambient noise would annihilate the pulse signals, which makes the instruments unable to reflect the real information of microparticles or inclusions. Therefore, reducing the interference of strong noise is the key technology to improve accuracy of the instruments.

In order to reduce the interference of strong noise, the previous solutions mainly used high--sensitive electronic components, electromagnetic shielding and grounding (Guthrie and Li, 2001). However, when the pulse signals are annihilated by noise, which means pulse amplitudes are less than the those of the noise, and the signal-to-noise ratio (SNR) of the signals satisfies SNR$\leqslant$ 0, modern signal processing technology cannot be used to identify weak signals with a low SNR. Weak signal detection has always been a research focus at home and abroad. Birx and Pipenberg (1992) used a chaotic oscillator to identify weak periodic signal for the first time. Since then, scholars studied the application of nonlinear systems to identify weak signal parameters. Chaotic oscillators had a very broad application in weak signal detection because

of their strong sensitivity to weak signals and good anti-noise capability (Feng *et al.*, 2012; Li H. *et al.*, 2022; Li J. *et al.*, 2014). On the other hand, the signals annihilated by noise can be reconstructed by a stochastic resonance of nonlinear system (Huang *et al.*, 2019). However, the signals detected in these previous studies are periodic signals.

Since Pecora and Carroll (1990) discovered chaotic synchronization, many achievements have been made in nonlinear synchronization (Duane *et al.*, 2017; Fu and Li, 2010; Goldobin and Pikovsky, 2005). Ye *et al.* (2009) studied a nonlinear response of Duffing oscillator to a chaotic sequence, found that the phases of the oscillator were positively correlated with the chaotic sequence. The study successfully detected an aperiodic electroencephalogram signal for the first time. Subsequently, the synchronization phenomenon in coupled oscillators excited by aperiodic signals has become a focus of study (Agrawal *et al.*, 2010; Anishchenko *et al.*, 2008; Baibolatov *et al.*, 2009; Ciszak *et al.*, 2009; Ott *et al.*, 2008). Inspired by the above research, Wu *et al.* (2011) studied the ring coupled Duffing oscillator excited by pulse signals in period-doubling bifurcation. They found that when one of the oscillators was excited by a pulse signal, the trajectory between oscillators changed from a synchronous state to an asynchronous state, and then returned to the synchronous state as the pulse passed. This phenomenon was defined as the transient synchronous mutation (TSM) phenomenon, based on which the existence of pulse signals annihilated by noise can be identified (Wu *et al.*, 2011a,b). These above researches mainly used the synchronous mutation of non-chaotic oscillators to identify aperiodic signals, and only verify the existence of pulse signals with a low SNR. Few research has been made to study the synchronous mutation of chaotic oscillators and their potential to identify the parameters of the signals.

This paper proposes an effective method to identify amplitudes of simulated Coulter signals with a low SNR by using the maximum difference ($\max(x_1 - x_2)$) between the state variables in the ring coupled double-Duffing (RCDD) oscillator with a chaotic state. The Coulter signals are measured by a Coulter counter, and a Gaussian pulse signal is used to simulate the Coulter signal, which is introduced into the RCDD oscillator. The identification function about $\max(x_1 - x_2)$ can be used to identify simulated Coulter signal amplitudes with a low SNR. Furthermore, the Simulink model of the RCDD oscillator is constructed, which verifies that the theoretical results can be applied to develop a technology for measuring Coulter signals with a low SNR, and promote the development of a nonlinear system in a measurement field.

2. Coulter signal and its simulated signal

Figure 1a is a schematic diagram of the Coulter Principle, opening a micropore on the side wall of a test tube, placing a pair of electrodes inside and outside the tube and putting them into a conductive solution. One end of the infusion tube is connected to the closed tube and the other end is connected to a pump to make the solution pass through the micropore. Applying direct current to both electrodes, the ESZ is formed near the micropore. When an insulated microparticle passes through the micropore with the solution, due to the conductivity difference between the microparticle and solution, the voltage between the two electrodes would change to form a pulse signal, which can reflect the size of the microparticle (Coulter, 1953). From Maxwell's equations, the pulse amplitude can be expressed as follows when the particle size is much smaller than the diameter of the micropore

$$\Delta U = \frac{4\rho_e I d^3}{\pi D^4} \tag{2.1}$$

where ρ_e is the resistivity of the conductive solution, d is the nominal size of the microparticle, D is the diameter of the micropore, I is the current through the micropore.

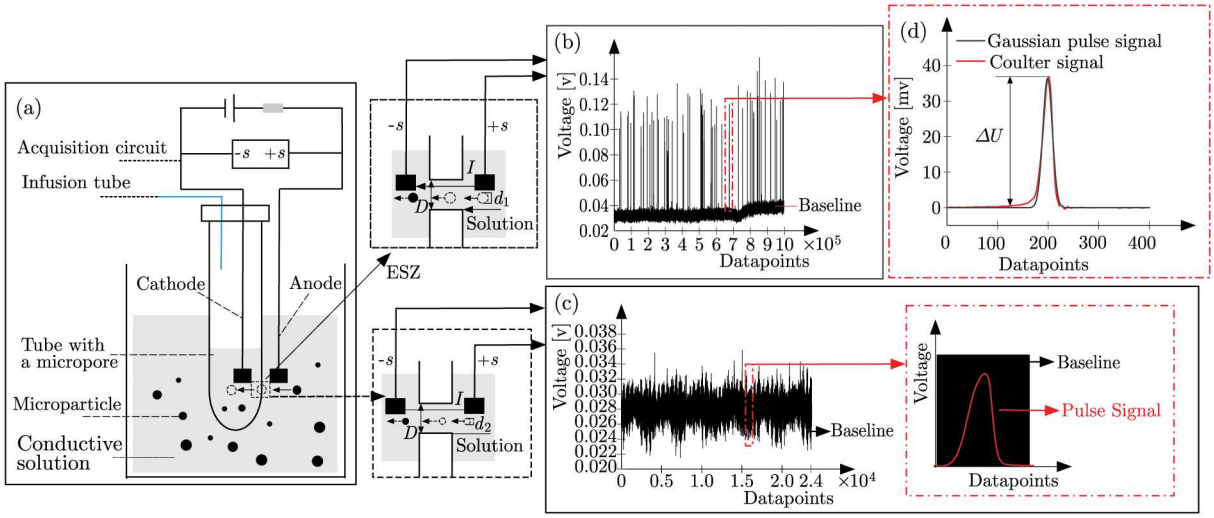

Fig. 1. (a) Schematic diagram of the ESZ method, (b) signals measured in the beaker containing microparticles with nominal size d_1, (c) signals measured in the beaker containing microparticles with nominal size d_2, (d) Gaussian pulse signal with proper parameters can mimic a Coulter signal

In the experiment of this paper, 0.9% saline was placed in two beakers with the same capacity, polystyrene standard particles with nominal sizes d_1 and d_2 were added to the two beakers, respectively, and the sizes of two microparticles met $d_1/D > d_2/D$. The real-time signals in different beakers at a stable speed in the magnetic stirrer were observed online by the Coulter counter respectively, as shown in Fig. 1b and 1c. By analyzing the measurement results, Coulter signals with obvious characteristics could be measured in the beaker containing the microparticles with size d_1. But the signals could not be measured in the beaker containing the microparticles with size d_2, because Coulter signals were annihilated in baseline. In order to improve the accuracy of the Coulter counter, Coulter signals annihilated by noise must be extracted.

In order to use chaotic oscillators to detect Coulter signals annihilated by noise, it is necessary to understand characteristics of the signals generated by microparticles with nominal size d_1. Wavelet denoising and morphological filtering were used to remove the noise in Coulter signals (Jagtiani *et al.*, 2008), and then we used the Gaussian pulse signal to simulate the Coulter signal. The function of the Gaussian pulse signal is $S_c(t) = r\exp\{-[(t-A)/B]2\}$, where r is the Gaussian pulse amplitude, A is the transient time corresponding to the Gaussian pulse peak, and B represents the dispersity of the signal, which determines width of the Gaussian pulse. Given proper values of A and B, a good fitting effect can be obtained, as shown in Fig. 1d. In this paper, white Gaussian noise is used to represent the noise in the measurement process. All the numerical experiments in this paper are prior, which means the parameters of Gaussian pulse signals are known, so as to find a method to identify parameters of pulse signals with a low SNR by using chaotic oscillators.

3. Investigation of parameters in a chaotic RCDD to study synchronous mutation

3.1. Amplitude selection of the driving force

In order to use the anti-noise ability of a chaotic Duffing system to identify amplitudes of simulated Coulter signals with a low SNR, this paper studies the synchronous mutation phenomenon in a chaotic RCDD system. The RCDD system is as follows (Wu *et al.*, 2011b)

$$\begin{aligned}\ddot{x}_1 + \xi\dot{x}_1 - x_1 + x_1^3 - k(x_2 - x_1) &= f\cos(\omega t) + S_c(t) + n(t)\\ \ddot{x}_2 + \xi\dot{x}_2 - x_2 + x_2^3 - k(x_1 - x_2) &= f\cos(\omega t)\end{aligned} \tag{3.1}$$

where ξ is the damping ratio, $f\cos(\omega t)$ is the periodic driving force. $k(x_i - x_j)$, $i \neq j$, $i, j \in \{1, 2\}$ is the coupling coefficient of the linear term between oscillators $(3.1)_{1,2}$, indicating the coupling strength between the two oscillators. $S_c(t)$ is the simulated Coulter signal and $n(t)$ is the white Gaussian noise. It is stated in the paper that when system (3.1) is chaotic, there would be no the TSM phenomenon (Wu *et al.*, 2011b). However, this is not true. In fact, the TSM phenomenon in chaotic oscillators can be controlled by setting proper parameters. We prove that the TSM phenomenon can still be observed in chaotic system (3.1) by setting different parameters in this paper.

In previous studies, when using a chaotic Duffing system to identify weak signal parameters, the damping ratio is generally selected as $\xi = 0.5$. Under different coupling coefficients, the amplitudes of the driving force are adjusted to make system (3.1) chaotic. Without a white Gaussian noise, setting parameters of system (3.1) as $\xi = 0.5$, $k = 0.1$, $\omega = 1$, the parameters of the simulated Coulter signal are $r = 0.25$, $A = 4$, $B = 1$, the calculation time of the numerical experiment is 100 s, the sampling interval is 0.01 s, and the initial value is [1,1,1,1]. The calculating time, sampling interval and initial value of all numerical experiments in this paper are the same, making the bifurcation diagram of system (3.1) changing with f, as shown in Fig. 2.

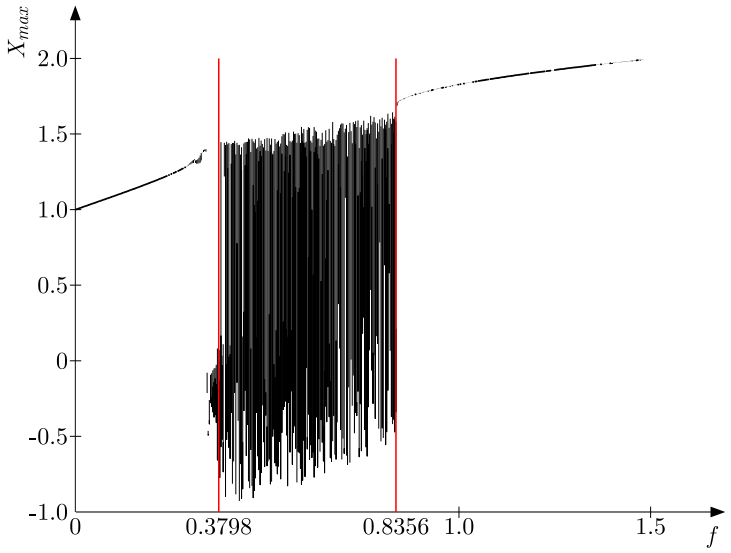

Fig. 2. Bifurcation diagram of system (3.1) via f

From Fig. 2, under a set of parameters, X_{max} label in the horizontal axis represents the maximum value of the phase trajectory of system (3.1) projected on the x-axis. If the phase of system (3.1) is periodic with the set of parameters, the number of X_{max} is finite. However, if the phase of system (3.1) is chaotic with the set of parameters, the number of X_{max} is infinite. Thus, when $k = 0.1$ and $f \in (0.3798, 0.8356)$, phases of system (3.1) are in chaos, as shown in Fig. 2. Then, combining with the controlling parameters of the nonlinear system, setting $k \in [0.1, 1]$ and making different bifurcation diagrams of system (3.1) changing with f, and selecting the intervals of f put system (3.1) in chaos. We find if f always takes a value from $(0.3896, 0.8301)$, system (3.1) is always chaotic. When k satisfies $k \in [0.1, 1]$, setting $f = 0.7 \in (0.3896, 0.8301)$, phases of oscillators $(3.1)_1$ and $(3.1)_2$ are shown in Fig. 3.

Through numerical simulations, when the parameters of system (3.1) satisfy $f = 0.7$ and $k \in [0.1, 1]$, the phases of the two oscillators are in a chaotic state, as shown in Fig. 3. When

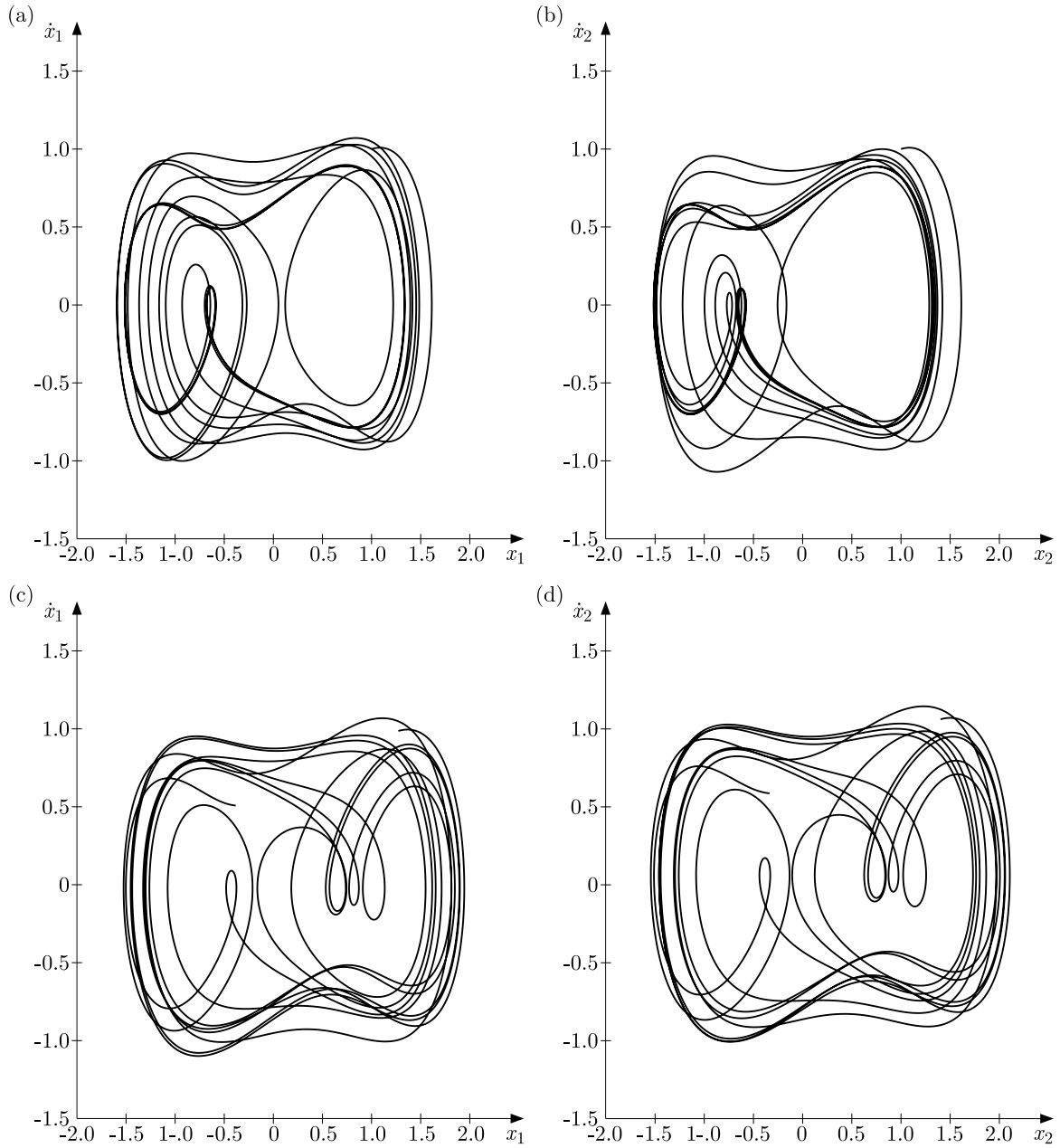

Fig. 3. Phase diagrams of system (3.1) with different values of k: (a) $k = 0.2$ – phase of oscillator $(3.1)_1$, (b) $k = 0.2$ – phase of oscillator $(3.1)_2$, (c) $k = 0.3$ – phase of oscillator $(3.1)_1$, (d) $k = 0.3$ – phase of oscillator $(3.1)_2$

$k = 0.2$, the phases of oscillators $(3.1)_1$ and $(3.1)_2$ are significantly different, so the two oscillators are in an asynchronous state, as shown in Fig. 3a and 3b. In contrast, when $k = 0.3$, the phases of oscillators $(3.1)_1$ and $(3.1)_2$ are only slightly different, which means that the two oscillators are in synchronization, as shown in Fig. 3c and 3d. Therefore, the values of the coupling coefficient determine whether the trajectories of the two oscillators are in synchronization or not.

3.2. Synchronous mutation phenomena with different values of k

Except that different coupling coefficients will affect the synchronization of the two oscillators, the solution interval will also affect the synchronous states (Woafo and Kraenkel, 2002). In this paper, when the interval is 0.01 s, the differences between the two state variables $x_1(t)$

and $x_2(t)$ in chaotic system (3.1) excited by the simulated Coulter signal are made to study the synchronous mutation phenomenon of system (3.1), and the values of k are selected from $[0.1, 1]$ to analyze the influence of different coupling coefficients on the phenomenon, as shown in Fig. 4.

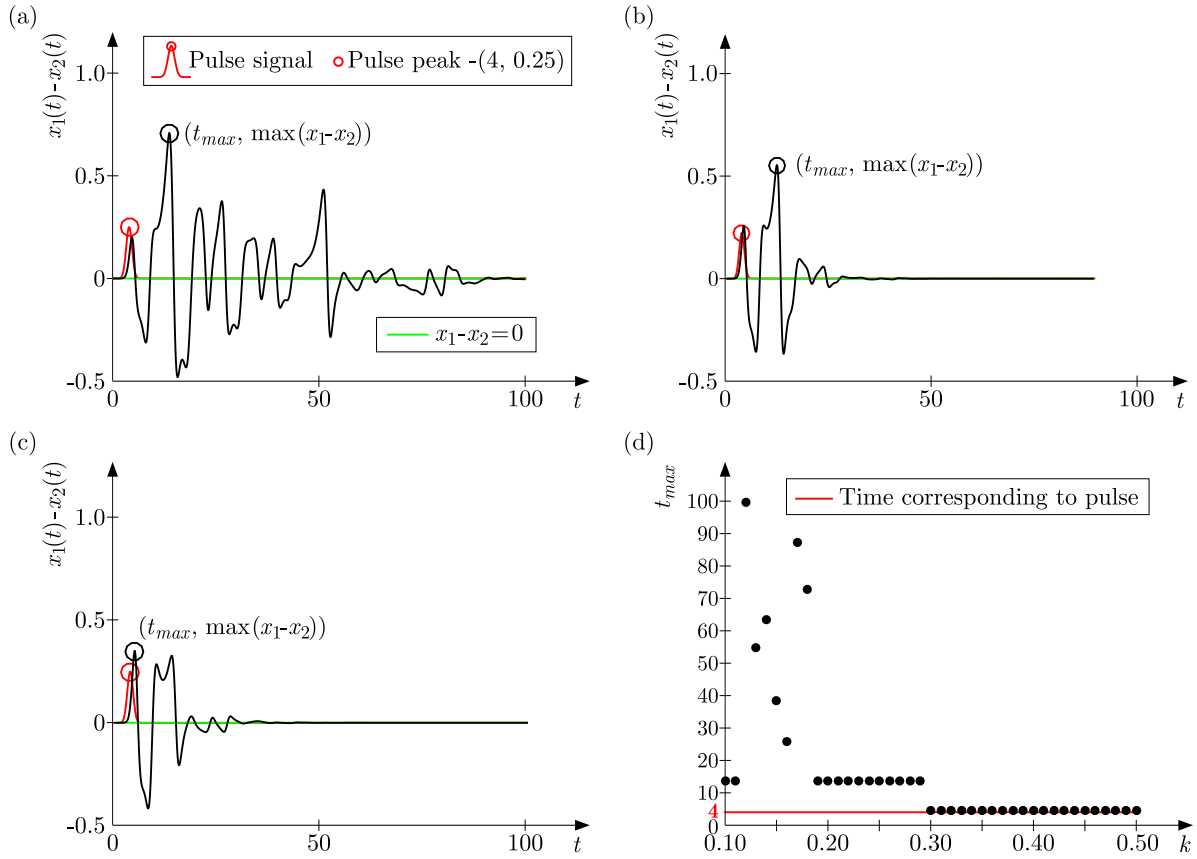

Fig. 4. (a) Synchronous mutation phenomenon with $k \in [0.1, 0.23)$, (b) synchronous mutation phenomenon with $k \in [0.23, 0.3)$, (c) synchronous mutation phenomenon with $k \in [0.3, 1]$, (d) different values of t_{max} with $k \in [0.1, 1]$

Figure 4 shows when k takes different values, the synchronous mutation phenomenon evolves gradually. When k satisfies $k \in [0.1, 0.23)$, the phenomenon persists in system (3.1), which means that the differences between the numerical solution $x_1(t)$ of oscillator $(3.1)_1$ and the numerical solution $x_2(t)$ of oscillator $(3.1)_2$ are not zero even after pulse passing, as shown in Fig. 4a. When k satisfies $k \in [0.23, 1]$, the TSM phenomenon is observed in Fig. 4b and 4c, which is due to the fact that the signal is limited and chaotic oscillators have inherent randomness, so that the two oscillators are synchronous as the signal disappears. When chaotic system (3.1) is excited by the signal and values of k belong to $[0.23, 1]$, the differences would change from a synchronous state to an asynchronous state. As the signal disappears, the differences would change from the asynchronous state to the synchronous state again, and keep staying in that state. This is defined as a chaotic transient synchronous mutation (C-TSM) phenomenon in this paper.

3.3. Reliability analysis of identifying the pulse based on the C-TSM phenomenon

Because values of k play an important role in controlling the synchronous mutation phenomenon in chaotic system (3.1), it is necessary to further analyze which value of k selected from $[0.1, 1]$ is more suitable for identifying simulated Coulter signals. It can be seen from Fig. 4 that there is a maximum value in the differences, which is defined as $\max(x_1 - x_2)$. The time

when $\max(x_1 - x_2)$ appears in Fig. 4 is always near 4 s corresponding to the pulse peak, which is defined as t_{max} . Therefore, it can be considered that $\max(x_1 - x_2)$ is caused by the pulse, and the closer $\max(x_1 - x_2)$ appears to the pulse peak, the higher reliability of $\max(x_1 - x_2)$ caused by the pulse. As shown in Fig. 4d, with an increase of k, values of t_{max} are gradually approaching the time 4 s.

When the coupling coefficient satisfies $k \in [0.3, 1]$, values of t_{max} are closer to 4 s than when the coupling coefficient is within $k \in [0.1, 0.3)$. According to the above parameter analysis, when k belongs to $[0.3, 1]$, the differences in system (3.1) exhibit the C-TSM phenomenon, which indicates that the C-TSM phenomenon is more suitable for identifying the pulses. Finally, the parameters of system (3.1) are determined as follows, the damping ratio is $\xi = 0.5$, the coupling coefficient is $k = 0.3$, and the amplitude of the driving force is $f = 0.7$. The influence of noise on the C-TSM phenomenon in chaotic system (3.1) is analyzed below.

4. Anti-noise ability of the RCDD system

4.1. Synchronization mutation phenomenon with noise

In the measurement experiment, there are various forms of noises in the environment, such as power frequency signals and interference signals similar to white noise, it is then necessary to understand the influence of noise on the C-TSM phenomenon. In this paper, white Gaussian noises with different variances are used to characterize the noise in the experiment, and the influence of the noises with different variances D on the C-TSM phenomenon are explored. Setting the variances as $D \in \{0.001, 0.01, 0.1, 1\}$, under the influences of noises, the differences between the two state variables $x_1(t)$ and $x_2(t)$ in chaotic system (3.1) excited by the simulated Coulter signal or not are made to study the synchronous mutation phenomenon, as shown in Fig. 5. From the noises with different variances and the signal with the same amplitude satisfying $r = 0.25$, we can calculate different values of the SNR.

It can be seen from Fig. 5 that under the influence of the noises, the C-TSM phenomena no longer exist in the differences, but the differences with or without the signal reveal continuous synchronous mutation phenomena, as shown by black solid lines or yellow dotted lines, respectively. The phenomenon is defined as a continuous synchronous mutation (CSM) in this paper, which means that the differences between $x_1(t)$ and $x_2(t)$ are always not zero. According to Fig. 5, there is still $\max(x_1 - x_2)$ in the CSM phenomenon with or without the signal, as shown by black circles or yellow circles, respectively.

Under the influence of noise with the same variance as in Fig. 5, by comparing t_{max} at 4 s as shown by the red circles, if there are no signals, t_{max} is relatively random, as shown by the yellow circles. Otherwise, values of t_{max} are always near the time 4 s, as shown by the black circles. Besides, $\max(x_1 - x_2)$ in the CSM phenomena with the signals is always greater than that without the signals, which means that $\max(x_1 - x_2)$ caused by the noise is not enough to exceed that caused by the signals. Therefore, with the influence of noise and signals, it can be considered that $\max(x_1 - x_2)$ is caused by the signal. Next, for different values of SNR, $\max(x_1 - x_2)$ is selected from the CSM phenomena in system (3.1) with a period-doubling bifurcation state or chaotic state. And the anti-noise ability of system (3.1) in the two states is analyzed.

4.2. Anti-noise ability of the RCDD system in the two states

Previous studies have explored the synchronous mutation phenomenon of system (3.1) in a period-doubling bifurcation. In order to analyze the anti-noise ability of system (3.1) in the period-doubling bifurcation or chaos, values of $\max(x_1 - x_2)$ are used to judge the stability of system (3.1) excited by simulated Coulter signals with and noise. The parameters are set as

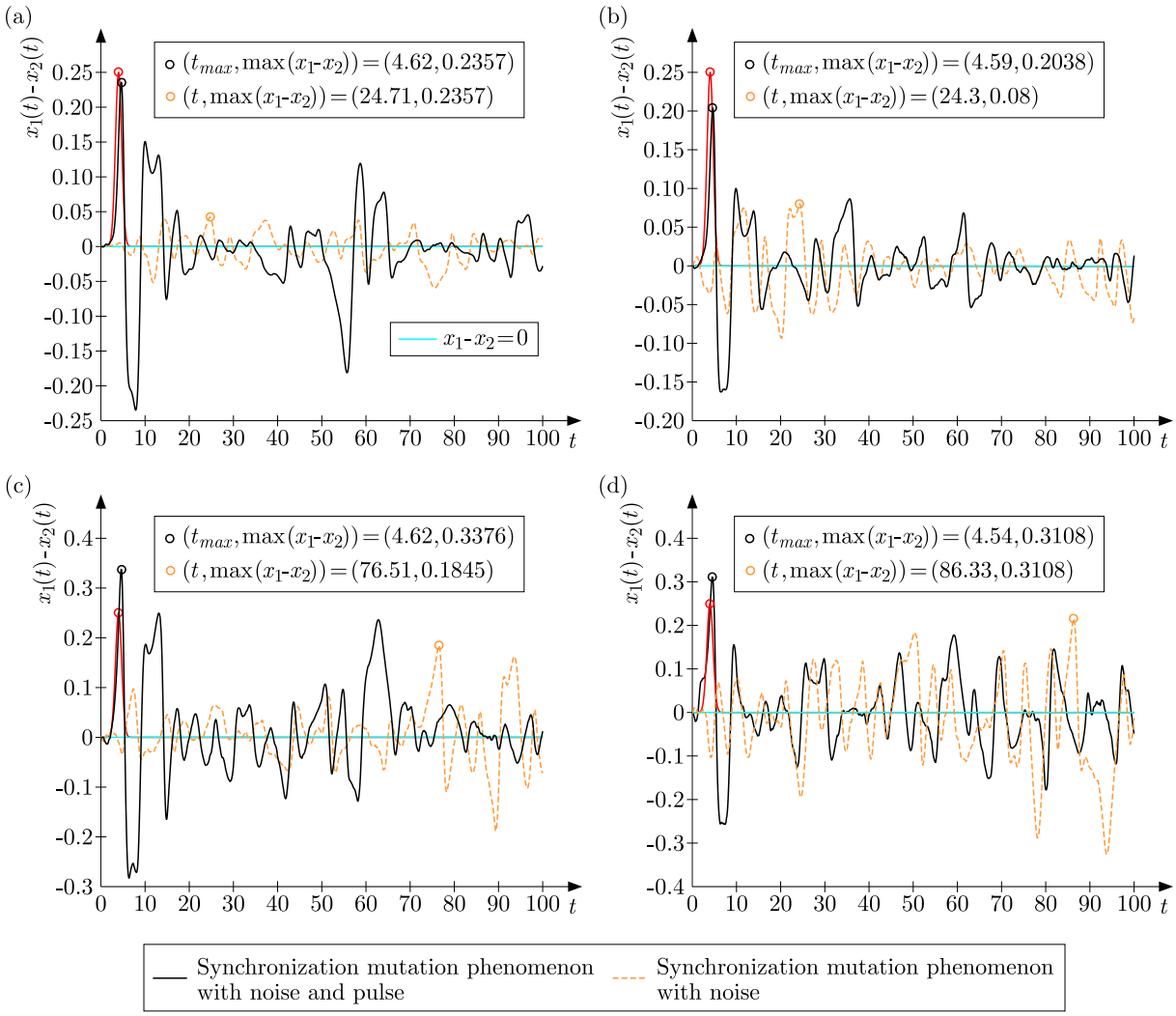

Fig. 5. Influence of noises with different variances, synchronization mutation phenomena in system (3.1) with or without pulse signal: (a) $D = 0.001$, SNR $= 41.4$ dB, (b) $D = 0.01$, SNR $= 18.3$ dB, (c) $D = 0.1$, SNR $= -4.7$ dB, (d) $D = 1$, SNR $= -27.7$ dB

$\xi = 0.35$, $k = 0.1$, $\omega = 1$, $f = 0.22$ according to Wu *et al.* (2011b), then system (3.1) would be in the period-doubling bifurcation. After adding the simulated Coulter signal to system (3.1), the synchronous mutation phenomenon with or without noise is shown in Fig. 6.

Without the noise, $\max(x_1 - x_2)$ is selected in the TSM phenomenon from Fig. 6a, which is redefined as $\max_{\text{PDB-TSM}} = 2.2459$. With the noise, system (3.1) has the CSM phenomenon as shown in Fig. 6b. From Fig. 4c, $\max(x_1 - x_2)$ is selected from the TSM phenomenon of chaotic system (3.1) without the noise, which is redefined as $\max_{\text{C-TSM}} = 0.19$.

When white Gaussian noises with different variances within $D \in \{0.001, 0.01, 0.1, 1\}$ and the signal are added to system (3.1), values of $\max(x_1 - x_2)$ appearing at around 4 s are selected from the CSM phenomena in system (3.1) with the period-doubling bifurcation or chaos, which is redefined as $\max_{\text{PDB-CSM}}$ or $\max_{\text{C-CSM}}$, respectively. Due to randomness of noise, the number of simulations for each variance is 100, and values of $\max_{\text{PDB-CSM}}$ or $\max_{\text{C-CSM}}$ selected each time are different. The anti-noise ability of system (3.1) in the period-doubling bifurcation or chaos is analyzed by changes of $\max_{\text{PDB-CSM}}$ ($\max_{\text{C-CSM}}$) compared with $\max_{\text{PDB-TSM}}$ ($\max_{\text{C-TSM}}$), as shown in Fig. 7.

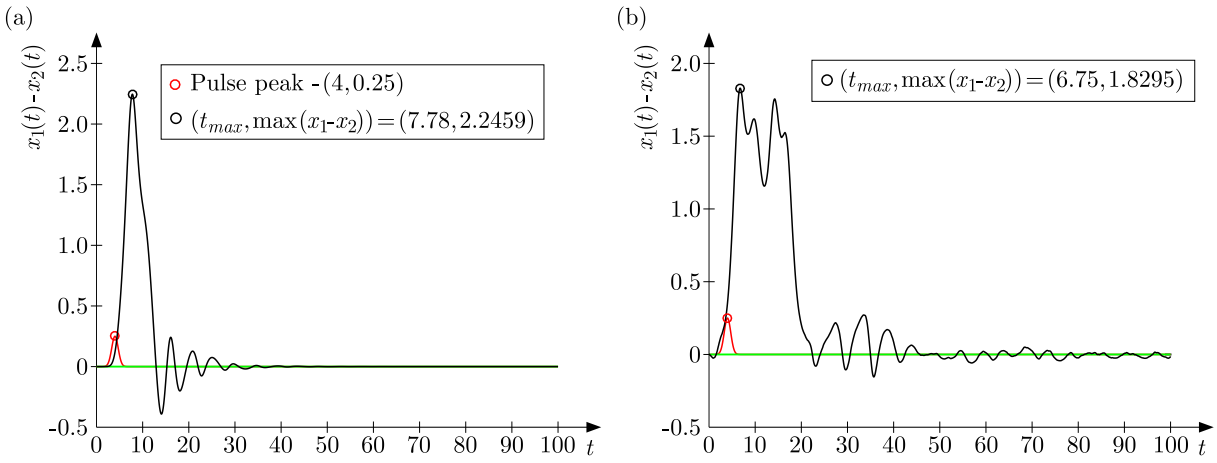

Fig. 6. Synchronous mutation phenomenon of system (3.1) in the period-doubling bifurcation: (a) without noise, (b) with noise

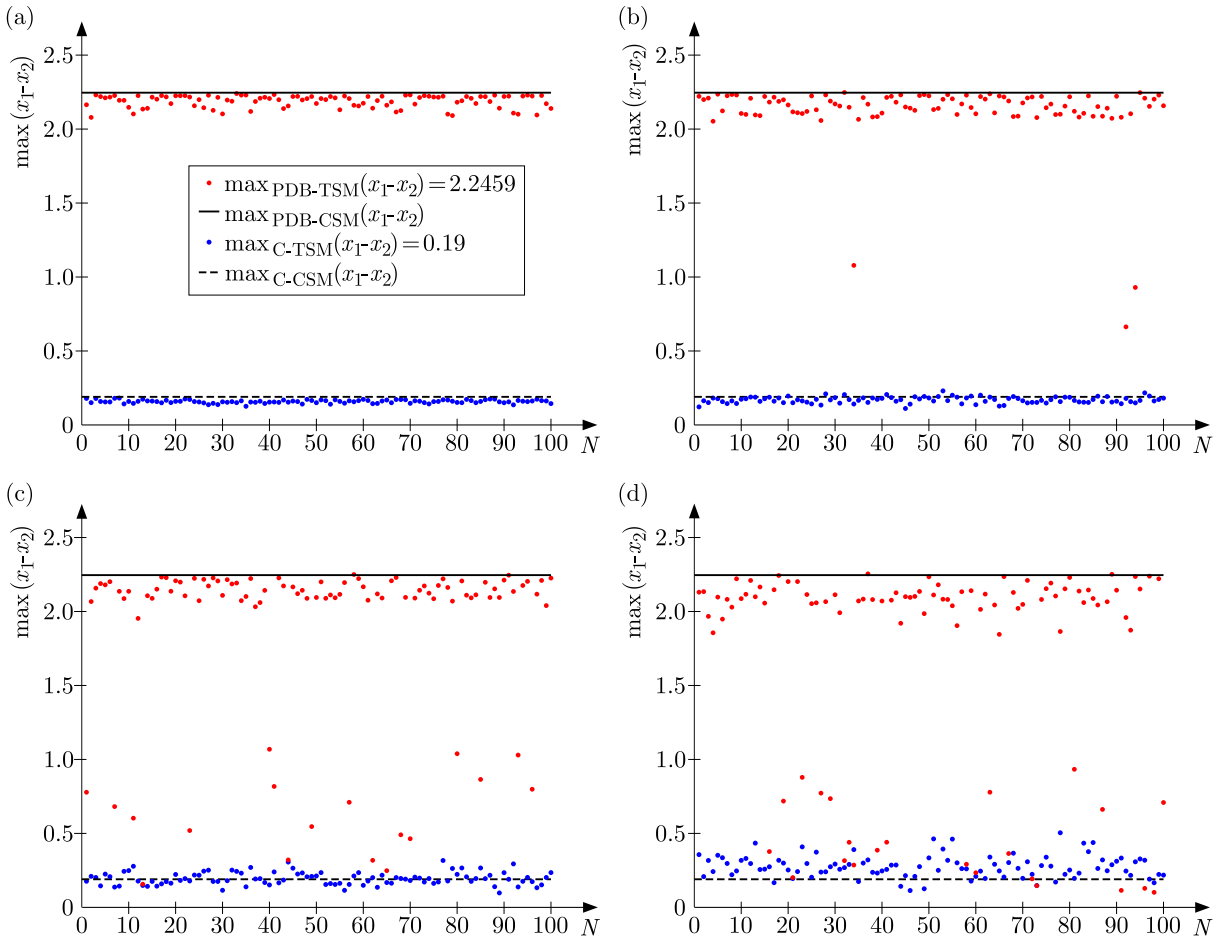

Fig. 7. Influence of noises with different variances and the signal, changes of $\max_{\text{PDB}-\text{CSM}}$ ($\max_{\text{C}-\text{CSM}}$) compared with $\max_{\text{PDB}-\text{TSM}}$ ($\max_{\text{C}-\text{TSM}}$): (a) $D = 0.001$, SNR = 41.4 dB, (b) $D = 0.01$, SNR = 18.3 dB, (c) $D = 0.1$, SNR = −4.7 dB, (d) $D = 1$, SNR = −27.7 dB

It can be seen from Fig. 7 that $\max_{\text{PDB}-\text{CSM}}$ or $\max_{\text{C}-\text{CSM}}$ would change compared with $\max_{\text{PDB}-\text{TSM}}$ or $\max_{\text{C}-\text{TSM}}$, which reflects the influence of noise on the stability of system (3.1). It can be seen from Fig. 7a and 7b that after being excited by the signal with a high SNR (SNR $>$ 0 dB), $\max_{\text{PDB}-\text{CSM}}$ ($\max_{\text{C}-\text{CSM}}$) slightly change compared with $\max_{\text{PDB}-\text{TSM}}$

($\max_{C-TSM}$), which shows that noise has little influence on the solutions of system (3.1) in the period-doubling bifurcation or chaos. As can be seen from Fig. 7c and 7d, after being excited by the signal with a low SNR, the changes of $\max_{C-CSM}$ compared with $\max_{C-TSM}$ are smaller than those of $\max_{PDB-CSM}$ compared with $\max_{PDB-TSM}$, which means that the solutions of chaotic system (3.1) are more stable than those of system (3.1) with the period-doubling bifurcation. Therefore, $\max_{C-CSM}$ can be better used to identify the simulated Coulter signals with a low SNR.

5. Identification of the pulse amplitude with a low SNR by using $\max(x_1 - x_2)$

Based on the above analysis, this paper uses $\max_{C-TSM}$ to identify amplitudes of the simulated Coulter signals with a low SNR. For convenience, $\max_{C-TSM}$ would be redefined as $\max(x_1 - x_2)$ in the rest of this paper. The signal amplitude is selected from $[0.01, 1]$, variance of noise set as $D = 1$ to make the SNR of the signal satisfy SNR $\leqslant 0\,\mathrm{dB}$, and values of $\max(x_1 - x_2)$ are selected from the CSM phenomena. Repeatedly setting signal amplitudes to obtain a large number of simulation data about $\max(x_1 - x_2)$, let $\max(x_1 - x_2)$ be an independent variable and the stated signal amplitude be a dependent one. The relationships between $\max(x_1 - x_2)$ and the stated amplitude are constructed by using different combinations of elementary functions and curve-fitting programs. Through a great deal of numerical simulations, the best relationship for identifying the amplitude is a polynomial function, as shown in equation (5.1), where $\widetilde{r}$ is the identified amplitude

$$\widetilde{r} = a_n \max(x_1 - x_2)^n + a_{n-1} \max(x_1 - x_2)^{n-1} + \cdots + a_1 \max(x_1 - x_2) + a_0 \tag{5.1}$$

We find that with an increase of the polynomial order, the identified amplitudes are closer to the stated pulse amplitudes. In this paper, a 6-degree polynomial function is used as the identification function to obtain amplitudes as shown in equation (5.2). The relationship between the simulation data and the identification function, and the errors between the stated amplitudes and identified amplitudes are shown in Fig. 8a and 8b, respectively

$$\begin{aligned}\widetilde{r} = {} & 0.1114 \max(x_1 - x_2)^6 - 2.6881 \max(x_1 - x_2)^5 + 9.9167 \max(x_1 - x_2)^4 \\ & - 14.5506 \max(x_1 - x_2)^3 + 9.0598 \max(x_1 - x_2)^2 - 1.0521 \max(x_1 - x_2) + 0.0987\end{aligned} \tag{5.2}$$

The errors between the identified amplitudes and stated amplitudes can not be obtained from Fig. 8a. Therefore, the proportion of the number of identified amplitudes within the allowable error in the total number of identified amplitudes is used to estimate the probability of equation (5.2) describing how effectively the amplitudes can be identified, see Fig. 8b. The simulation results show that when the allowable error is 15%, the probability of equation (5.2) to identify amplitudes is only $\sim 48\%$, which is due to large errors when identifying the amplitudes with a low SNR. Under the influence of noise with variance $D = 1$, different stated amplitudes are set to obtain different values of the SNR and identification functions. When the allowable error is 15%, the probabilities that the functions can effectively identify the amplitudes are obtained with different values of the SNR, as shown in Table 1.

It can be seen from Table 1 that when the allowable error is 15%, as the interval of the stated amplitude or SNR shrinks, the probability of identification functions to identify amplitudes increases. If the interval of the stated amplitude is within $[0.5, 1]$, the probability can be improved to 80%, and the identification function is constructed as shown in equation (5.3), which can be used with the lowest SNR at about $-13.86\,\mathrm{dB}$

$$\begin{aligned}\widetilde{r} = {} & -22.7025 \max(x_1 - x_2)^6 + 106.7767 \max(x_1 - x_2)^5 - 197.5111 \max(x_1 - x_2)^4 \\ & + 181.2927 \max(x_1 - x_2)^3 - 85.5568 \max(x_1 - x_2)^2 + 19.7986 \max(x_1 - x_2) - 1.215\end{aligned} \tag{5.3}$$

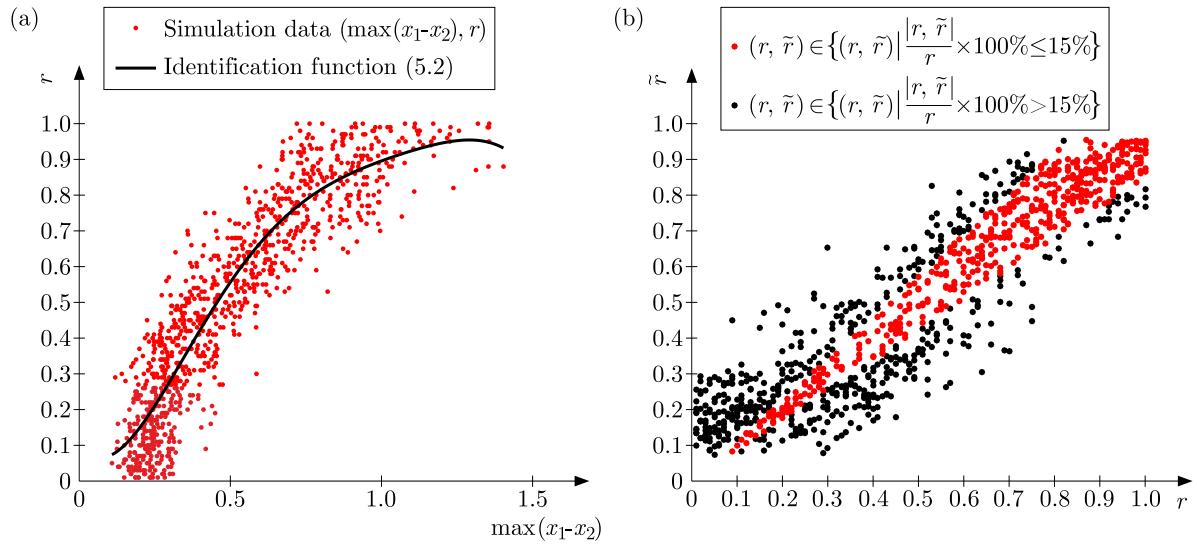

Fig. 8. (a) Simulation data and identification function (5.2), (b) errors between identified amplitudes and stated amplitudes

Table 1. Probability of different identification functions to identify amplitudes with different stated amplitudes or values of SNR

Interval of stated amplitude or SNR	Total number of identified amplitudes	Number of identified amplitudes satisfied $\lvert r-\tilde{r}\rvert/r \leqslant 15\%$	Probability
$[0.01, 1]/[-92.1\,\mathrm{dB}, 0\,\mathrm{dB}]$	1000	482	48.2%
$[0.1, 1]/[-46.05\,\mathrm{dB}, 0\,\mathrm{dB}]$	910	479	52.64%
$[0.2, 1]/[-32.19\,\mathrm{dB}, 0\,\mathrm{dB}]$	810	483	59.63%
$[0.3, 1]/[-24.08\,\mathrm{dB}, 0\,\mathrm{dB}]$	710	491	69.15%
$[0.4, 1]/[-18.33\,\mathrm{dB}, 0\,\mathrm{dB}]$	610	456	74.75%
$[0.5, 1]/[-13.86\,\mathrm{dB}, 0\,\mathrm{dB}]$	510	406	79.61%
$[0.6, 1]/[-10.22\,\mathrm{dB}, 0\,\mathrm{dB}]$	410	343	83.66%
$[0.7, 1]/[-7.13\,\mathrm{dB}, 0\,\mathrm{dB}]$	310	276	89.03%
$[0.8, 1]/[-4.46\,\mathrm{dB}, 0\,\mathrm{dB}]$	210	208	99.05%
$[0.9, 1]/[-2.11\,\mathrm{dB}, 0\,\mathrm{dB}]$	110	110	100%

6. Simulink model of the RCDD system

In order to verify if $\max(x_1 - x_2)$ selected from the CSM phenomenon can be used to identify amplitudes of simulated Coulter signals with a low SNR, a Simulink model of system (3.1) has been designed in Matlab. Rewriting system (3.1), one obtains

$$\begin{aligned} \dot{x}_1 &= y_1 \qquad & \dot{y}_1 &= -\xi y_1 + x_1 - x_1^3 + k(x_2 - x_1) + f\cos(\omega t) + \widetilde{s}_c(t) + \sqrt{D}\widetilde{n}(t) \\ \dot{x}_2 &= y_2 \qquad & \dot{y}_2 &= -\xi y_2 + x_2 - x_2^3 + k(x_1 - x_2) + f\cos(\omega t) \end{aligned} \tag{6.1}$$

The parameters in system (6.1) are $\xi = 0.5$, $\omega = 1$ and $f = 0.7$, respectively, and the coupling coefficient is still selected from the interval $[0.1, 1]$, which is taken as $k = 0.9$. $\widetilde{s}_c(t)$ and $\widetilde{n}(t)$ in system (6.1) represent the simulated Coulter signal and noise respectively, and the parameters of the signal are $r = 0.5$, $A = 4$ and $B = 1$. System (6.1) is constructed by using a Matlab/Simulink module, as shown in Fig. 9.

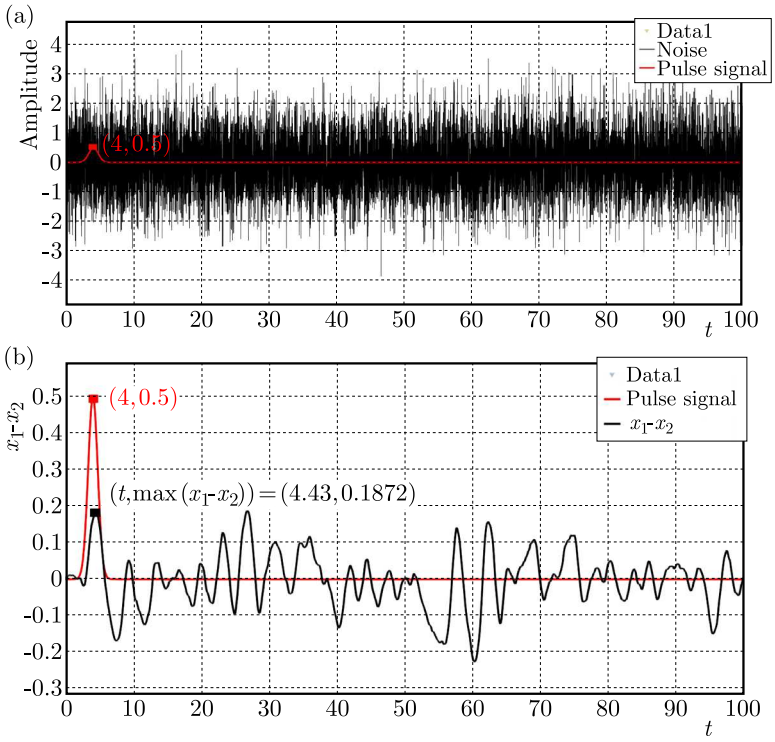

Fig. 9. Simulink model of system (6.1)

In the simulation model, Sine Waves 1 and 2 represent the driving force in system (6.1). Random Number represents the noise $\widetilde{n}(t)$. The module constructed by the Clock and Interpreted MATLAB functions represents the simulated Coulter signal. Gains 1 and 3 represent coupling coefficients k, and Gains 2 and 4 represent damping ratios ξ. The definitions of other modules can be found in Matlab/Simulink. The simulation time and sampling interval of the model are 100 s and 0.01 s, respectively, which are the same as the calculation time and sampling interval of the previous numerical simulations. Firstly, parameters of each module in the model are set according to the parameters of system (6.1), and the Random Number module is closed to verify whether the state and the synchronous mutation phenomenon in the model are consistent with the above simulation results of system (3.1) without the noise. From the output results of the modules XY graph1 and Scope, the phase of oscillator $(6.1)_1$ and the differences between the two state variables x_1 and x_2 are observed respectively, as shown in Fig. 10.

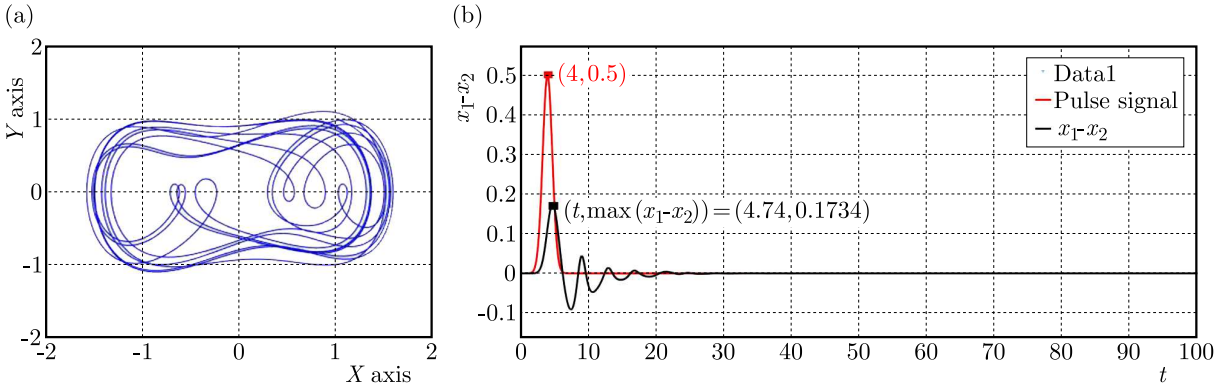

Fig. 10. (a) Phase of oscillators $(6.1)_1$ from XY graph1, (b) C-TSM phenomenon from Scope

It can be seen from Figs. 3 and 10 that phases of oscillators $(3.1)_1$ and $(6.1)_1$ are both in the chaotic state, and both differences in systems (3.1) and (6.1) reveal the C-TSM phenomena. t_{max} (4.74 s) is close to 4 s corresponding to the pulse peak, which shows that $\max(x_1 - x_2)$ in the C-TSM phenomenon of system (6.1) is caused by the pulse. Secondly, the parameters of the Random Number module as Mean = 0, Variance = 1 are set to generate the noise. The signal composed of the pulse and noise is observed by module Scope1, and its SNR is −13.86 dB, as shown in Fig. 11.

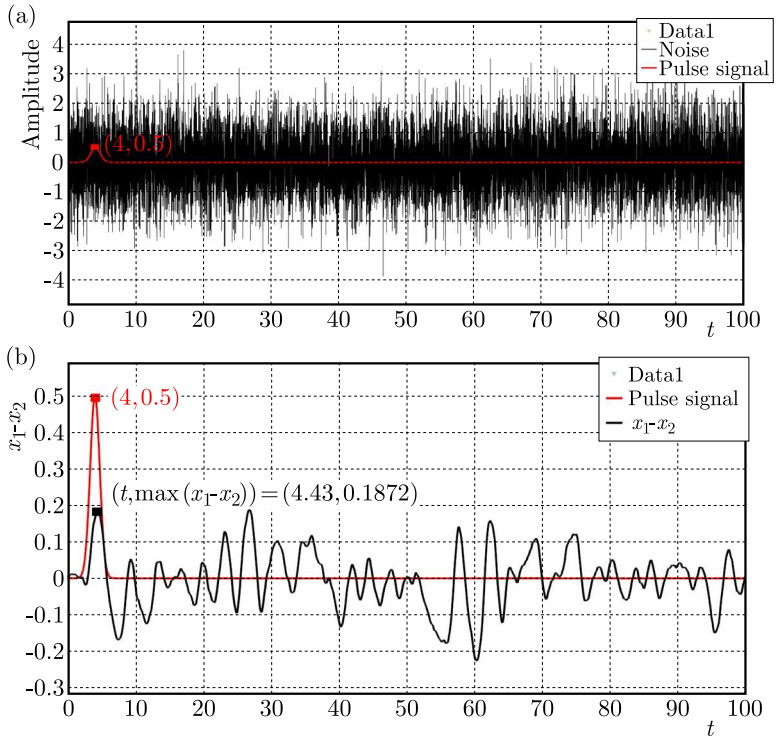

Fig. 11. (a) The signal composed of the pulse and noise from Scope1, (b) CSM phenomenon from Scope

As shown in Fig. 11a, the pulse has been annihilated by the noise. Scope is used to observe the synchronous mutation phenomenon in system (6.1) and to extract $\max(x_1 - x_2)$, as shown in Fig. 11b. Under the influence of noise, the differences have the CSM phenomenon in system (6.1), and t_{max} (4.43 s) is close to 4 s. The value of $\max(x_1 - x_2)$ selected from Fig. 11b is 0.1872 is substituted into equation (5.3) to obtain the identified amplitude $\widetilde{r} = 0.4634$. The relative error between the identified and stated amplitude is $|\widetilde{r} - r|/r \cdot 100\% = |0.4634 - 0.5|/0.5 \cdot 100\% \approx 7.3\%$. From the simulation results, it is verified that $\max(x_1 - x_2)$ in the CSM phenomenon can be used to identify the amplitude of the simulated Coulter signal with a low SNR. Meanwhile, Simulink model of system (6.1) lays the foundation for building of an electronic circuit of the RCDD system. However, parameters (e.g. amplitude and width) of Coulter signals represent physical processes and are unknown. The next study would build the electronic circuit of the RCDD system applyied to carry out a measurement experiment for detecting Coulter signals with a low SNR.

7. Conclusions

In order to use chaotic oscillators to identify amplitudes of Coulter signals with a low SNR (SNR$\leqslant$ 0), a Gaussian pulse signal is used to simulate the Coulter signal, and the synchronous mutation phenomenon of the chaotic ring coupled double-Duffing (RCDD) oscillator is studied. It is found that if the coupling coefficient is $k \geqslant 0.23$, there will appear a chaotic-transient

synchronous mutation (C-TSM) phenomenon in the oscillator excited by the simulated Coulter signal. Moreover, the maximum difference ($\max(x_1 - x_2)$) in the C-TSM phenomenon is caused by the signal. After being excited by a signal and white Gaussian noise, a continuous synchronous mutation (CSM) phenomenon occurs in the oscillator, and $\max(x_1 - x_2)$ is still caused by the signal. Under different values of SNR, $\max(x_1 - x_2)$ is selected from the CSM phenomena of the oscillator in the period-doubling bifurcation or chaos respectively, and the changes of $\max(x_1 - x_2)$ are analyzed to explore better anti-noise ability of the chaotic oscillator for a low SNR. Subsequently, $\max(x_1 - x_2)$ is used as an independent variable to construct a function to identify the simulated Coulter signal amplitude with a low SNR. The proportion of the number of identified amplitudes within the allowable error in the total number of identified amplitudes is used to estimate the probability that the function can effectively identify the amplitudes, and the lowest SNR for identification by making use of this function is -13.68 dB. A simulink model of the oscillator is constructed to verify that the values of $\max(x_1 - x_2)$ in the CSM phenomenon can be used to identify amplitudes of simulated Coulter signals with a low SNR, and it lays the foundation for study of the electronic circuit of the oscillator. The results in this paper show that the CSM phenomenon in the RCDD oscillator can be used to develop a technology for measuring Coulter signals with a low SNR.

Acknowledgements

This study was financially supported by the Beijing City Science and Technology Bureau; The Huairou Science City Achievements Implementation Special Project (Grant No. Z201100008420010); The Science and Technology Innovation Fund of Weiqiao-UCAS (Grant No. 20D101652DY) and the 'Double First-Class' Construction Fund (Grant No. 111800XX62) which greatly acknowledged.

References

1. Agrawal M., Prasad A., Ramaswamy R., 2010, Quasiperiodic forcing of coupled chaotic systems, *Physical Review E*, **81**, 2, 026202
2. Anishchenko V., Nikolaev S., Kurths J., 2008, Bifurcational mechanisms of synchronization of a resonant limit cycle on a two-dimensional torus, *Chaos: An Interdisciplinary Journal of Nonlinear Science*, **18**, 3, 037123
3. Baibolatov Y., Rosenblum M., Zhanabaev Z.Z., Kyzgarina M., Pikovsky A., 2009, Periodically forced ensemble of nonlinearly coupled oscillators: From partial to full synchrony, *Physical Review E*, **80**, 4, 046211
4. Birx D.L., Pipenberg S.J., 1992, Chaotic oscillators and complex mapping feed forward networks (CMFFNS) for signal detection in noisy environments, *Proceedings of the International Joint Conference on Neural Networks (IJCNN)*
5. Ciszak M., Montina A., Arecchi T., 2009, Control of transient synchronization with external stimuli, *Chaos: An Interdisciplinary Journal of Nonlinear Science*, **19**, 1, 015104
6. Coulter W.H., 1953, *Means for Counting Particles Suspended in a Fluid*, U.S. Patent 2,656,508
7. Doutre D., 1984, The development and application of a rapid method of evaluating molten metal cleanliness, Ph.D.Thesis, McGill University, Montreal
8. Duane G.S., Grabow C., Selten F., Ghil M., 2017, Introduction to focus issue: Synchronization in large networks and continuous media – Data, models, and supermodels, *Chaos: An Interdisciplinary Journal of Nonlinear Science*, **27**, 126601
9. Feng J., Zhang Q., Wang W., 2012, Chaos of several typical asymmetric systems, *Chaos, Solitons and Fractals*, **45**, 7, 950-958
10. Fu G.-Y., Li Z.-S., 2010, Adaptive synchronization of a hyperchaotic Lü system based on extended passive control, *Chinese Physics B*, **19**, 6, 060505

11. Goldobin D.S., Pikovsky A., 2005, Synchronization and desynchronization of self-sustained oscillators by common noise, *Physical Review E*, **71**, 4, 045201

12. Guthrie R.I.L., Li M., 2001, In situ detection of inclusions in liquid metals: Part II. Metallurgical applications of LiMCA systems. *Metallurgical and Materials Transactions B*, **32**, 6, 1081-1093

13. Huang D., Yang J., Zhou D., Sanjuán M.A.F., Liu H., 2019, Recovering an unknown signal completely submerged in strong noise by a new stochastic resonance method, *Communications in Nonlinear Science and Numerical Simulation*, **66**, 156-166

14. Jagtiani A., Sawant R., Carletta J., Zhe J., 2008, Wavelet transform-based methods for denoising of Coulter counter signals, *Measurement Science and Technology*, **19**, 6, 065102

15. Li H., Tian R., Xue Q., Zhang Y., Zhang X., 2022, Improved variable scale-convex-peak method for weak signal detection, *Chaos Solitons and Fractals*, **156**, 111852

16. Li J., Zhang L., Wang D., 2014, Unique normal form of a class of 3 dimensional vector fields with symmetries, *Journal of Differential Equations*, **257**, 7, 2341-2359

17. Ott E., Platig J.H., Antonsen T.M., Girvan M., 2008, Echo phenomena in large systems of coupled oscillators, *Chaos: An Interdisciplinary Journal of Nonlinear Science*, **18**, 3, 037115

18. Pecora L.M., Carroll T.L., 1990, Synchronization in chaotic systems, *Physical Review Letters*, **64**, 8, 821-824

19. Woafo P., Kraenkel R.A., 2002, Synchronization: Stability and duration time, *Physical Review E*, **65**, 3, 036225

20. Wu Y., Zhang S., Sun J., Rolfe P., 2011a, Abrupt change of synchronization of ring coupled Duffing oscillator, *Acta Physica Sinica – Chinese Edition*, **60**, 2

21. Wu Y., Zhang S., Sun J., Rolfe P., Li Z., 2011b, Transient synchronization mutation of ring coupled Duffing oscillators driven by pulse signal, *Acta Physica Sinica – Chinese Edition*, **60**, 10, 100509-100501

22. Ye Y., Yue L., Mandic D., Bao-Jun Y., 2009, Regular nonlinear response of the driven Duffing oscillator to chaotic time series, *Chinese Physics B*, **18**, 3, 958-968

Manuscript received December 20, 2022; accepted for print January 12, 2023